Papers

Influence of Carrier Nonuniformity on the Phase Relationship Between Frequency and Intensity Modulation in Semiconductor Lasers

OWEN DOYLE, PHILIPPE B. GALLION, MEMBER, IEEE, AND GUY DEBARGE

Abstract—**The chirp to modulated power ratio is an important characteristic of semiconductor laser dynamics and is closely related to the linewidth enhancement factor α. We have measured the modulus and phase of the CPR for a 1.5 μm buried heterostructure laser and a 0.85 μm channeled-substrate planar (CSP) laser. The results for the phase are inconsistent with previously published expressions including spontaneous emission and spectral hole burning. In particular the CSP laser exhibits an abrupt phase shift in the CPR. We present an explanation of this behavior in terms of the influence of a nonuniform carrier density on the phase-amplitude coupling, as expressed by an integral expression for the mode parameter α. Using a simple model for lateral behavior which analytically incorporates diffusion and a nonuniform material α parameter, we obtain qualitative agreement with the CSP data. Thus we demonstrate the importance of the lateral laser structure on the phase-amplitude coupling in index-guided semiconductor lasers, and the usefulness of CPR phase measurements for laser characterization.**

I. Introduction

THE coupling between the phase and amplitude of the optical field in a semiconductor laser is manifest in a wide variety of laser characteristics such as linewidth, phase noise, injection locking bandwidth, and the extent of chirp. In many practical cases, in particular at high frequencies, the dominant source of this coupling is the joint carrier density dependence of the real and imaginary parts of the refractive index, a relationship commonly parameterized by the linewidth broadening factor, α [1], [2].

The chirp to modulated power ratio, or CPR, is a very simple way to measure the phase-amplitude coupling for a single-mode laser [3]. In the sinusoidal steady state, the CPR is the ratio of the complex amplitudes of optical frequency and power variations, generally expressed in GHz/mW. Its modulus measures the extent of chirp for a given power variation, and its phase equals the phase angle between the simultaneous intensity and frequency modulations. In addition to being a very useful parameter for the study of phase-amplitude coupling by canceling the parasitic electrical response of the laser and drive circuit, as well as relaxation resonance effects, the CPR is directly pertinent to the design of single-mode optical communications systems.

Recent theoretical calculations of the linear, small-signal CPR, including the effects of spontaneous emission and gain suppression (due to spectral hole burning) can be summarized by the following expression [3], [4]:

$$\mathrm{CPR} = \frac{\alpha}{2P_o}\left(jf_{\mathrm{mod}} + C_1P_o + \frac{C_2}{P_o}\right) \qquad (1)$$

where P_o is the output power per facet in mW and f_{mod} is the modulation frequency in GHz. The parameters C_1 and C_2 are given by

$$C_1 = \frac{\epsilon\Gamma}{h\nu \cdot \pi\eta V} \qquad C_2 = \frac{\eta P_{\mathrm{spon}}}{4\pi\tau_p}$$

in which $h\nu$ is the photon energy, η the external efficiency, V the active region volume, Γ the confinement factor, and τ_p the photon lifetime. P_{spon} is the spontaneous power in the laser mode, and ϵ is the gain suppression factor (in m^3).

The extreme simplicity of (1) at high modulation frequencies, for which the first term dominates, suggests a straightforward technique for measuring α. More generally, if (1) accurately describes laser behavior, precise measurements may lead to values for parameters such as the gain suppression factor [5].

The measurements described in Section II yield results consistent with (1) with respect to the CPR modulus, but strikingly different in its phase. An explanation of the observed behavior for the CSP laser is presented in Section III, based on an analytical model of lateral mode and carrier nonuniformity in the laser cavity.

II. CPR Measurement

Determining the CPR requires knowledge of the intensity modulation (IM) and frequency modulation (FM) characteristics of a laser. The spectrum under direct sinusoidal modulation is predominantly FM, with an asymmetry introduced by intensity modulation. Thus it is possible, given the IM index, to extract both the frequency modulation depth and CPR phase angle from the analysis of dynamic spectra under weak modulation. This simple technique has been discussed previously [6].

Manuscript received September 8, 1987.

The authors are with the Ecole Nationale Supérieure Télécommunications, 75634 Paris Cedex 13, France.

IEEE Log Number 8718669.

The intensity modulation index for a given bias current, as a function of the nominal RF power of the sinusoidal modulating current and the modulation frequency, was determined by observing the optical output with increasing sinusoidal excitation at 100 MHz. At low excitation levels, corresponding to low IM indexes, the optical waveform is sinusoidal, its amplitude increases proportionally to the excitation (square root of RF power), and the average optical power is constant. As the excitation is increased, the onset of clipping in the optical waveform, the rolloff in relative optical response and the rise in dc optical power all indicate the point at which the IM index equals unity. Independently, the IM response was measured as a function of frequency, remaining in the sinusoidal regime. Assuming a linear relationship between the sinusoidal current and intensity amplitudes, these two measurements allow one to determine the IM index at a given bias current for any excitation power or frequency. This value is used in the analysis of the corresponding spectrum, yielding the FM index and IM/FM phase delay. The power was generally chosen to give first-order FM sidebands with intensities roughly 0.2 to 0.3 relative to the main peak. The corresponding IM indexes were on the order of 0.1 to 0.2.

This technique has been applied to two very different lasers: 1) a Hitachi HLP1400 AlGaAs channeled-substrate planar laser ($\lambda = 0.83\ \mu m$) and 2) a CNET distributed-feedback, InGaAsP, buried heterostructure laser ($\lambda = 1.52\ \mu m$). The results for each laser at several output powers are shown in Figs. 1 and 2.

The dynamic spectrum tends toward symmetry at high frequencies, corresponding to a CPR phase angle of $\Psi = \pm\pi/2$. (This ambiguity is inherent in the simple technique, as described previously.) The value was chosen in accordance with the high frequency value of (1), i.e., $\Psi = \pi/2$. This choice lifted the ambivalence for the CNET BH laser. However, for the Hitachi CSP laser, the asymmetry attains a maximum, corresponding unambiguously to $\Psi = \pi$, at a frequency which depends on the power; as the frequency is lowered below this point, the spectrum again tends toward symmetry, and no assumptions can be made about the low-frequency asymptote. At every dc power level, the spectrum reaches this critical asymmetry, and we have consequently chosen the CPR phase such that its slope is continuous at this point. The flat regions near this value result from slight errors in the IM index, precluding a real solution to the analytical equations at the extrema of spectral asymmetry.

The modulus of the CPR for both lasers can be approximately described by (1). Despite the dispersion in the data at high frequencies, due to the difficulties in obtaining precise values for the IM indexes, values of $\alpha = 6.2$ for the Hitachi laser and $\alpha = 7.9$ for the CNET laser provided reasonable fits to the slopes of the CPR modulus at all powers for each laser. For comparison, the values deduced from the linewidth versus inverse power curves (using for the CNET laser the expression for DFB lasers neglecting facet reflectivity [7]) are $\alpha = 5.7$ for the Hitachi laser and $\alpha = 6.4$ for the CNET laser. We note that the CPR measurements provide a more direct, and hence potentially more accurate measure of α than does the linewidth. In principle the gain suppression factor can be derived by fitting the nonlinear CPR modulus to (1), but more accurate measurements are necessary to obtain a good estimate. Without sufficient precision to make a detailed comparison, we can nonetheless conclude that (1)

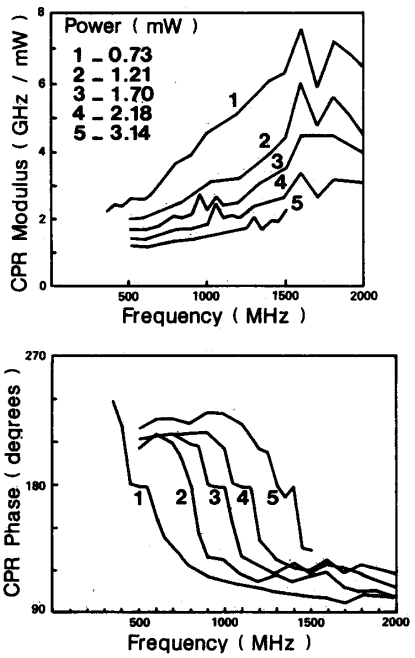

Fig. 1. Modulus and phase of the CPR for a Hitachi HLP1400 laser measured at several output powers.

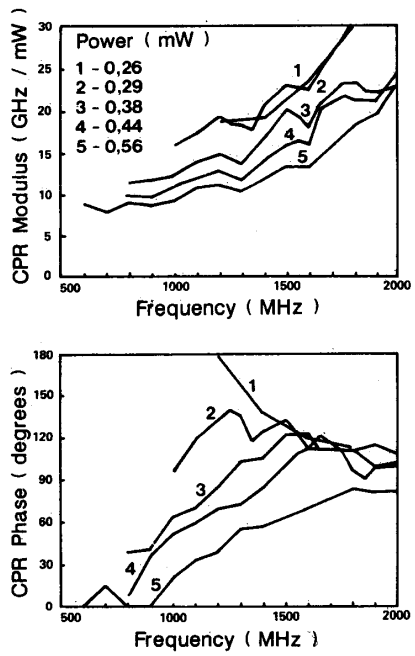

Fig. 2. Modulus and phase of the CPR for a 1.5 μm buried heterostructure DFB laser (CNET).

is entirely sufficient to describe qualitatively the modulus of the CPR.

In contrast, it can be seen that the phase of the CPR, which according to (1) should vary slowly between 0 and $\pi/2$, is not correctly described. We conclude that the phase is more sensitive than the modulus to certain device characteristics which are not taken into account in the models leading to (1). For the CNET BH laser, the phase at high output powers is qualitatively in agreement with (1), while a significant deviation occurs at low power. The Hitachi CSP laser shows even greater divergence from the prediction, with an abrupt phase shift passing through $\Psi = \pi$. This divergence corroborates the observation of Harder *et al.* [8], who found a frequency-sensitive linewidth enhancement factor for CSP lasers. Previous measurements of the FM response, such as those of Jacobsen *et al.* [9], have given the current-to-FM phase, which exhibits a 180° phase shift at the relaxation oscillation frequency. Such a phase shift is not related to the shift observed here (the relaxation oscillation effects are canceled in the CPR). However, Sudbø [10] measured the phase relationship between the intensity and frequency modulations for the same type of laser several years ago, and his results show a similar phase shift, although the asymptotes differ from ours. We will focus on the results for the CSP laser, proposing an analysis in which lateral nonuniformity is used to explain the observed phase behavior qualitatively, with rough quantitative agreement. The approach is very similar to those of Nilsson and Yamamoto [11] and Kikuchi *et al.* [12], [13], who applied simple nonuniform models to explain anomalies in the FM response. Our measurements of the CPR allow a thorough analysis along the lines of these works.

III. Lateral Analysis

To study the nonuniform case, we must distinguish between local, constitutive parameters, and overall mode parameters. We will consider a local material definition of the coupling parameter, denoted α_L, a function of the carrier density n and optical frequency ω [14] (with change of notation):

$$\alpha_L(\omega, n) = -\frac{d\epsilon'(\omega, n)/dn}{d\epsilon''(\omega, n)/dn} \tag{2}$$

where $\epsilon = \epsilon' + j\epsilon''$ is the complex optical dielectric constant. The modal phase-amplitude coupling can be described by the general expression [1]

$$\dot{\phi} = \frac{\alpha}{2}\frac{\dot{I}}{I_o} \tag{3}$$

which relates the variations in phase and intensity of a single-mode laser field via a general coupling parameter α. For a uniform cavity, considering only carrier-induced changes in optical response, $\alpha = \alpha_L$, a constant. In the general case, including for example, gain suppression, the coupling is more complex and cannot be described by a time-independent coefficient in (3). However, (3) may still be useful as a concise expression of the coupling, with a generalized parameter $\alpha(t)$.

It is recognized that a large number of factors contribute to the α of (3) [2], [15]. In order to focus our attention on the influence of the carrier and optical mode profiles within the cavity, we will neglect spontaneous emission and spectral hole burning (which can be expressed through $\alpha(t)$ in (3), although such is not the clearest way to include them). The latter neglect may significantly weaken the agreement of our model with the measured data, as we shall see, but the inclusion of gain suppression at this point would make it virtually impossible to evaluate the direct influence of lateral structure, which is our goal. In index-guided lasers, perturbation analysis of the waveguide equation leads then to the expression [8], [15], [16]

$$\alpha(t) = \frac{\int |E_o(x)|^2 \cdot \alpha_L(x) \cdot \Delta\epsilon''(x, t)\, dx}{\int |E_o(x)|^2 \cdot \Delta\epsilon''(x, t)\, dx} \tag{4}$$

where $E_o(x)$ is the normalized steady-state field profile, and $\Delta\epsilon''(x, t)$ is the carrier-induced variation in the imaginary part of the dielectric constant. This expression is equivalent to that given by Harder *et al.* [8] and is described in detail by Sudbø [15], [16], who gives the more general expression including wavefront curvature along with the corresponding field normalization conditions. As an approximation, we can apply (4) independently in the two coordinates perpendicular to the axis of propagation. In the transverse direction, perpendicular to the junction plane, the relative uniformity of the field and carriers through the thin active layer and the absence of excitation outside this region ($\Delta\epsilon'' = 0$ while $E_o \neq 0$) simplifies the equation, with no consequence for α. Very thin active layers may lead to gain-guiding effects and wavefront curvature, significantly modifying α [17], [18], but these are neglected in (4). We limit our study to lateral behavior across the active layer, denoted by the coordinate x.

Two special cases of (4) are worth note. First, if α_L is uniform, then $\alpha = \alpha_L$ regardless of the field and excitation profiles. However, it is known that at a fixed frequency, $\alpha_L(n)$ increases with carrier density [14], [2], and will therefore be spatially dependent if the steady-state carrier profile is nonuniform. Second, if the time dependence and spatial dependence of the excitation are separable, i.e., $\Delta\epsilon''(x, t) = \Delta\epsilon''(x) \cdot f(t)$, then α is reduced to a time-independent, space-averaged value. A nonuniform steady-state carrier distribution leads to spatially-dependent modulation via the operating point for the local rate equations. To the extent that the experimental results for the CPR phase are inconsistent with a constant α [1], these two special cases should be critically examined.

To test the hypothesis that the CPR phase anomaly for the Hitachi laser is a result of the lack of lateral carrier confinement in the CSP structure, a simple model of lateral behavior was developed. We have incorporated an

analytical treatment of carrier diffusion, and have the significant advantage of the elimination of electrical response and relaxation oscillation effects inherent to the definition of the CPR.

The optical mode profile in the cold cavity is assumed known, given the mode and guide widths. (It is taken as the solution to the one-dimensional wave equation with a real index step.) The region of analysis was limited such that the neglected power, in the wings of the optical mode, is one one-tenth of the total power. The configuration is symmetric, and each half is divided into two zones, defined by x_1 and x_2, containing equal energy (or power since the group index is nearly constant laterally), as shown in Fig. 3. The parameters of the model are the average photon density S in the combined regions, the phase ϕ of the mode, and the average carrier densities n_1 and n_2 in each region. The average photon densities in each region are given by $\xi_1 S$ and $\xi_2 S$, where ξ_1 and ξ_2 depend on the respective volumes and hence on the form of the optical mode: in particular $\xi_1 = 0.45 \cdot x_2/x_1$ and $\xi_2 = 0.45 \cdot x_2/(x_2 - x_1)$ (10 percent of power neglected).

The standard rate equations describing this laser model are

$$\begin{aligned}
\dot{S} &= \left[\Gamma g(n_1 - n_o) + \Gamma g(n_2 - n_o) - 1/\tau_p\right] \cdot S \\
\dot{n}_1 &= J_1 - n_1/\tau_n - g(n_1 - n_o)\xi_1 S \\
\dot{n}_2 &= J_2 - n_2/\tau_n - g(n_2 - n_o)\xi_2 S \\
\dot{\phi} &= \tfrac{1}{2}\Gamma g(\alpha_1 \cdot \delta n_1 + \alpha_2 \cdot \delta n_2)
\end{aligned} \tag{5}$$

where g is the linear gain coefficient, n_o is the local transparency density, τ_p the photon lifetime, and τ_n the carrier lifetime. Γ is an equivalent confinement factor, equal by construction to $0.45 \cdot \Gamma_y$ where Γ_y is the standard transverse confinement factor. J_i is the density of carrier injection in the ith region, and α_i the local α_L parameter, function of the steady-state value of n_i. The phase variation (ignoring a constant frequency shift) is expressed in terms of the carrier density excursions δn_i from their steady-state values. This coupled system of equations is solved in the steady state and then linearized to analyze small-signal modulation behavior.

The incorporation of diffusion is given special attention. We wished to avoid both a fully numerical treatment, in which diffusion is part of the original equations and solution proceeds by a finite element method, and analytical approximations which begin with nonphysical carrier and mode profiles. In our treatment, diffusion introduces explicit relationships between the carrier densities of each region, as described below.

We assume a uniform carrier injection of density J_o on $-d < x < d$, and we begin by calculating the carrier distribution in the absence of an optical field. The solution to this simple steady-state diffusion problem yields a proportionality between J_o and the average carrier density n_i in each zone:

$$n_i = (J_o \tau_n) \cdot D_{io} \qquad i = 1, 2. \tag{6}$$

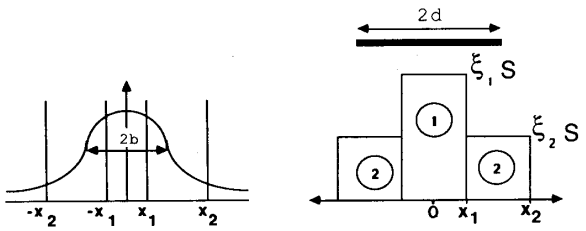

Fig. 3. Schematic of the partition of the active layer used to model lateral behavior. The optical mode is deduced from the guide width and mode width ($2b$) using the symmetric dielectric waveguide equations without gain.

The coefficients designated D_{io} are functions of x_1, x_2, and d. These relations are valid for all J_o less than the threshold density J_o^t, at which the carrier densities are n_1^t and n_2^t. Above threshold, the carrier density distribution is modified by the field, while the overall average density remains constant as in the uniform case (with the approximations of this model). Writing $n_i = n_i^t + \Delta n_i$, the steady-state equivalent of (5) can be written

$$\begin{aligned}
&n_1^t + \Delta n_1 - n_o + n_2^t + \Delta n_2 - n_o = 1/(\tau_p \Gamma g) \\
&D_{1o}(J_o - J_o^t) - g(n_1^t + \Delta n_1 - n_o) \\
&\quad \cdot \xi_1 S - \Delta n_1/\tau_n = 0 \\
&D_{2o}(J_o - J_o^t) - g(n_2^t + \Delta n_2 - n_o) \\
&\quad \cdot \xi_2 S - \Delta n_2/\tau_n = 0.
\end{aligned} \tag{7}$$

Here we have approximated the effective carrier density injection in each region by (6), although the carrier distribution is slightly modified.

At threshold, $\Delta n_1 = \Delta n_2 = 0$, and above threshold, from the first term in (7), $\Delta n_1 = -\Delta n_2$. From these equations then, the threshold values can be calculated. Above threshold, the steady-state carrier densities n_{1o} and n_{2o} and the average photon density S_o can be given as functions of J_o.

The incorporation of diffusion into the dynamic behavior is based on the classical diffusion equation for $n(x, t)$:

$$\frac{dn}{dt} = -\frac{n}{\tau_n} + D\frac{d^2 n}{dx^2} + J(x, t) \tag{8}$$

where D is the diffusion coefficient. A single spontaneous lifetime τ_n is used, neglecting stimulated emission at this step. This approach, while very approximate, is consistent with commonly accepted diffusion lengths on the order of a few microns, for D roughly 100 cm^2/s (see parameter list below). The Green's function solution to this equation is

$$n(x, t) = \frac{e^{-t/\tau_n}}{(4\pi D t)^{1/2}} e^{-x^2/4Dt}. \tag{9}$$

Therefore, the response at all x and t to a uniform injection in the region i at $t = 0$ is

$$h_i(x, t) = \frac{e^{-t/\tau_n}}{(4\pi Dt)^{1/2}} \frac{1}{V_i} \int_{V_i} e^{-(x-x')^2/4Dt}\, dx' \quad (10)$$

where V_i is the one-dimensional volume of the region. We take diffusion into account by considering dn_i/dt as a source whose solution is (10). That is, any variation in the average carrier density of the region i modifies the densities everywhere at later times. Hence

$$dn(x, t)/dt = dh_i(x, t)/dt \otimes dn_i/dt \quad (11)$$

where $\otimes$ represents temporal convolution. The final step is an integration over each region j to obtain the averages appropriate for the model:

$$\frac{dn_j}{dt} = \frac{1}{V_j} \int_{V_j} \frac{dh_i(x, t)}{dt} \otimes \frac{dn_i}{dt}\, dx \equiv D_{ij} \otimes \frac{dn_i}{dt}. \quad (12)$$

These diffusion-related sources are added to the external injection sources, leading to the following substitutions in (5):

$$J_i \rightarrow J_i + D_{ii} \otimes n_i + D_{ij} \otimes n_j. \quad (13)$$

The calculation of D_{ij} is shown in the Appendix. Note that $D_{ii} < 0$ and for $i \neq j$, $D_{ij} > 0$ and $V_i \cdot D_{ij} = V_j \cdot D_{ji}$, as one should expect.

In order to calculate the CPR, the system of equations must be linearized, given the steady-state solution, and transformed into the frequency domain ($S = S_o + \tilde{S}e^{j\Omega t}$, etc.). This straightforward procedure leads to the following system of equations:

$$\begin{aligned} &j\Omega\tilde{S} - \Gamma g S_o \tilde{n}_1 - \Gamma g S_o \tilde{n}_2 = 0 \\ &\xi_1 g(n_{1o} - n_o)\tilde{S} - [j\Omega(1 - \tilde{D}_{11}) + 1/\tau_n + \xi_1 g S_o] \\ &\quad \cdot \tilde{n}_1 - j\Omega\tilde{D}_{12}\tilde{n}_2 = \tilde{J}_1 \\ &\xi_2 g(n_{2o} - n_o)\tilde{S} - j\Omega\tilde{D}_{21}\tilde{n}_1 \\ &\quad - [j\Omega(1 - \tilde{D}_{22}) + 1/\tau_n + \xi_1 g S_o]\tilde{n}_2 = \tilde{J}_2. \end{aligned} \quad (14)$$

$\tilde{J}_1$ and $\tilde{J}_2$ are simply the averages over each region, given x_1, x_2, and d, of the sinusoidally-varying injected carrier densities. Dynamic diffusion is expressed by the $\tilde{D}_{ij}$, rather than as coefficients for the sources, in contrast to the steady-state solution. The coefficients $\tilde{D}_{ii}$ represent the diffusion of carriers out of the region i, naturally including diffusion away from the optical mode.

The phase equation is simply

$$j\Omega\tilde{\phi} = \tfrac{1}{2}\alpha_1 \Gamma g \tilde{n}_1 + \tfrac{1}{2}\alpha_2 \Gamma g \tilde{n}_2 \quad (15)$$

and the CPR is by definition

$$\text{CPR} \equiv \frac{j\Omega\tilde{\phi}}{2\pi\tilde{P}} \quad (16)$$

in which $\tilde{P}$ is the sinusoidal power variation per facet

$$\tilde{P} = h\nu(\tfrac{1}{2}\eta/\tau_p) V_m \tilde{S} \quad (17)$$

where V_m is the modal volume. In the present case, given the active region thickness L_y, the laser length L_z, and the lateral partition described above, the modal volume is $V_m = 2x_2 \cdot L_y \cdot L_z/(0.9\Gamma_y)$.

The third-order system of (14) is solved as a function of modulation frequency for $\Omega/2\pi$ between 100 MHz and 2 GHz, and the expressions (15)–(17) are used to calculate the model CPR in this frequency range, over which the experimental observations were made.

The following parameters were used in the model: $\eta = 0.5$, $\tau_n = 2.0$ ns, $\tau_p = 1.7$ ps, $n_o = 1.3 \times 10^{18}$ cm^{-3}, $\Gamma_y = 0.2$. The physical dimensions are $L_z = 300$ μm, $L_y = 0.15$ μm, a guide width of 4.0 μm and a mode width of 5.0 μm, yielding $x_1 = 1.0$ μm and $x_2 = 2.7$ μm. The gain coefficient was $g = 3.7 \times 10^{-6}$ s^{-1} cm^3, determined from the relaxation oscillation freuqencies, whose squares increase linearly with power with a slope of 2.19 GHz/mW. Given a diffusion coefficient of $D = 100$ cm^2/s, the resultant damping of relaxation oscillations reduced the resonance peaks in the IM response of the model from the undamped case, fitting quite well the observed IM responses between 0.5 and 3 mW. The value of $\alpha_1 = 5.7$ was determined from the linewidth of the laser, measured by the self-heterodyne technique [19] as 150 MHz · mW. This is an approximation for the sake of obtaining a reasonable numerical value, since the actual linewidth depends on the full carrier and mode profiles just as the CPR does. The ratio α_2/α_1 was varied between 0 and 2, with the relationship between α_1 and n_{io} being considered *a posteriori*.

Fig. 4 shows the calculated CPR for $\alpha_2/\alpha_1 = 0.5$ and $d = 1$ μm. Despite the crudeness of the numerical application (only two zones), the results provide clear evidence of the effects of lateral structure. The high-frequency slopes of the modulus for different powers agree well with the measured values. Most importantly, the CPR phase shows an abrupt transition in qualitative agreement with the measured phase [in contrast with Eq. (1)]. Moreover, this transition has the proper power dependence. Two discrepancies are clear however: the direction of the phase shift and the precise transition frequencies.

While graphically striking, the first discrepancy can be readily explained and is in fact minor. It is clear that the imaginary part of the CPR dominates everywhere above 100 MHz, and that it is a change in sign of this imaginary part which yields the transition. This dominance of the imaginary part is consistent with a uniform model in which spontaneous emission and gain suppression are neglected: in that case the CPR is purely imaginary, while the inclusion of gain suppression introduces a real part. In our model, the real part is too small (the modulus approaches zero when the imaginary part changes sign). In addition, this real part has the wrong sign (the phase passes through 0 rather than π, as observed), but being so close to 0, its sign cannot be considered significant. The real part of the CPR in our model appears therefore to be primarily a numerical artifact, and hence the direction of variation in the phase should not be taken as significant. It seems quite

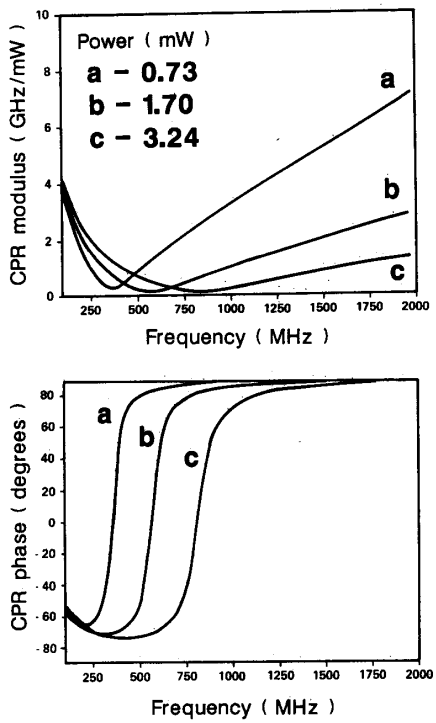

Fig. 4. Modulus and phase of the CPR for the model presented, calculated for the same optical powers as in Fig. 1.

plausible that the inclusion of gain suppression in the nonuniform model would generate a real part consistent with the measured phase values.

The frequency at which the phase shifts depends strongly on the stripe width, on the ratio α_2/α_1, and in certain cases on the diffusion coefficient. The principle effect of the latter is through the steady-state carrier distribution. The ratio α_2/α_1 should be consistent with the carrier densities (i.e., $\alpha_2 < \alpha_1$ for $n_{2o} < n_{1o}$ which is the case here). However, only a narrow stripe width in the model gave transition frequencies reasonably close to those observed. This may be related to the crudeness of the two-zone partition, calling for an increase in the number of zones.

Nonetheless, several important conclusions concerning lateral behavior in a semiconductor laser can be drawn from the present simple analysis. First, for $\alpha_1 = \alpha_2$, the CPR phase for the model is $\pi/2$ at all frequencies, as can be seen immediately by combining (15) with the top term in (14). The phase is thus strongly influenced by nonuniformity in the material α_L parameter. Second, a dephasing (i.e., different time dependence) between the carrier density modulations in the two zones is responsible for the CPR phase shift. This is seen by observing the phases of $\tilde{n}_1$, $\tilde{n}_2$, $\tilde{\phi}$ and $\tilde{S}$ with respect to the excitation. All of them exhibit the expected phase shift at the relaxation oscillation frequency, which cancels out in the CPR. An additional shift in $\tilde{\phi}$, qualitatively arising from different phase behavior in $\tilde{n}_1$ and $\tilde{n}_2$, is the direct source of the shift in the CPR phase. Both of these conditions, that α_L be nonuniform and that the carrier modulation be of spatially-variable phase, are in fact consequences of the general conclusions concerning the origins of time dependence in α described above. Moreover, both of these can be traced to a nonuniform carrier density.

IV. Conclusion

By measuring the phase, as well as the modulus, of the chirp to modulated power ratio for two different laser types, we have observed discrepancies with previously published theoretical expressions. We have provided a qualitative explanation for a Hitachi HLP1400 laser in terms of lateral nonuniformity in the laser cavity. In particular, the model developed incorporates carrier diffusion and a nonuniform material "linewidth enhancement factor," α_L. The observed variations in the CPR phase are seen to be consequences of the time dependence of the general phase-amplitude coupling factor α. Complete measurement of the CPR is thus shown to be a useful tool in laser characterization. In particular, the phase is very sensitive to the carrier distribution and may be used to study the latter. Conversely, the conditions of carrier confinement must be recognized as important in determining the relationship between the frequency and intensity modulation characteristics of a semiconductor laser.

Appendix

We evaluate the coefficient D_{11}, defined by (9)–(12), and give the result for the other coefficients. The D_{ij} for $i = 1$ concerns a source assumed uniform over $|x| \leq x_1$ (see Fig. 3). The normalized response to such a source, at all points of the model, is

$$h_1(x, t) = \frac{e^{-t/\tau_n}}{(4\pi Dt)^{1/2}} \frac{1}{2x_1} \int_{-x_1}^{x_1} e^{-(x-x')^2/4Dt}\, dx'.$$

The time derivative is

$$\frac{dh_1}{dt} = \frac{-h_1}{\tau_n} + \frac{e^{-t/\tau_n}}{8x_1 t(\pi Dt)^{1/2}} \cdot \left[(x - x_1)e^{-(x-x_1)^2/4Dt} - (x + x_1)\, e^{-(x+x_1)^2/4Dt}\right]$$

from which we calculate the coefficient $D_{11}(t)$

$$D_{11}(t) = -\frac{[n_1]}{\tau_n} + \frac{e^{-t/\tau_n} D^{1/2}}{x_1(4\pi t)^{1/2}} \left[e^{-x_1/Dt} - 1\right].$$

The term $[n_1]$ simply represents the integral on V_1 of the response to the source in V_1. Convolved with this source, the term leads to a contribution n_1/τ_n which expresses carrier recombination in the region. This contribution appears in all the D_{ij}, but it is already explicitly included in the rate equations, and is dropped from the coefficients of diffusion. The three other coefficients are calculated similarly. They are transformed into the frequency domain

using the integral

$$\int_0^\infty e^{-j\Omega t}\frac{e^{-t/\tau_n}}{t^{1/2}}e^{-\tau'/t}\,dt = \left(\frac{\pi}{1/\tau + j\Omega}\right)^{1/2}\exp\left[-2(1/\tau + j\Omega)^{1/2}\tau'^{1/2}\right].$$

The dynamic diffusion length L_Ω is defined by

$$L_\Omega = \left(\frac{D}{1/\tau + j\Omega}\right)^{1/2}.$$

The coefficients of dynamic diffusion are finally

$$\tilde{D}_{11}(\Omega) = -\frac{L_\Omega}{2x_1}\left(1 - \exp\left(-2x_1/L_\Omega\right)\right)$$

$$\tilde{D}_{12}(\Omega) = -\frac{L_\Omega}{2x_1}\left(1 - \exp\left(-2x_1/L_\Omega\right) - \exp\left(-(x_2 - x_1)/L_\Omega\right) + \exp\left(-(x_2 + x_1)/L_\Omega\right)\right)$$

$$\tilde{D}_{21}(\Omega) = \frac{x_1}{x_2 - x_1}\tilde{D}_{12}(\Omega)$$

$$\tilde{D}_{22}(\Omega) = -\frac{L\Omega}{2(x_2 - x_1)}\left(1 - \tfrac{1}{2}\exp\left(-2x_1/L_\Omega\right) - \tfrac{1}{2}\exp\left(-2x_2/L_\Omega\right) - \exp\left(-(x_2 - x_1)/L_\Omega\right) + \exp\left(-(x_2 + x_1)/L_\Omega\right)\right).$$

Acknowledgment

The authors would like to thank J. C. Bouley and A. Scavenec of the CNET for supplying the DFB laser and the high-speed detector used for the 1.5 μm measurements.

References

[1] C. H. Henry, "Theory of the linewidth of semiconductor lasers," *IEEE J. Quantum Electron.*, vol. QE-18, pp. 259-264, 1982.
[2] M. Osiński and J. Buus, "Linewidth broadening factor in semiconductor lasers—An overview," *IEEE J. Quantum Electron.*, vol. QE-23, pp. 9-29, 1987.
[3] T. L. Koch and J. E. Bowers, "Nature of wavelength chirping in directly modulated semiconductor lasers," *Electron. Lett.*, vol. 20, pp. 1038-1040, 1984.
[4] R. S. Tucker, "High-speed modulation of semiconductor lasers," *J. Lightwave Technol.*, vol. LT-3, pp. 1180-1192, 1985.
[5] C. B. Su, V. Lanzisera, and R. Olshansky, "Measurement of nonlinear gain from FM modulation index of InGaAsP lasers," *Electron. Lett.*, vol. 21, pp. 893-894, 1985.
[6] O. Doyle, "Measuring modulus and phase of chirp/modulated power ratio," *Electron. Lett.*, vol. 23, pp. 133-134, 1987.
[7] K. Kojima and K. Kyuma, "Analysis of the spectral linewidth of distributed feedback laser diodes," *Electron. Lett.*, vol. 20, pp. 869-871, 1984.
[8] C. Harder, K. Vahala, and A. Yariv, "Measurement of the linewidth enhancement factor of semiconductor lasers," *Appl. Phys. Lett.*, vol. 42, pp. 328-330, 1983.
[9] A. S. Sudbø, "Direct measurement of the frequency-modulation characteristics of a coupled-cavity laser," *IEEE J. Quantum Electron.*, vol. 20, pp. 88-89; erratum, p. 271, 1984.
[10] G. Jacobsen, H. Olesen, F. Birkedahl, and B. Tromborg, "Current/frequency modulation characteristics for directly optical frequency-modulated injection at 830 nm and 1.3 μm," *Electron. Lett.*, vol. 18, pp. 874-876, 1982.
[11] O. Nilsson and Y. Yamamoto, "Small-signal response of a semiconductor laser with inhomogeneous linewidth enhancement factor: Possibilities of a flat carrier-induced FM response," *Appl. Phys. Lett.*, vol. 46, pp. 223-225, 1985.
[12] K. Kikuchi, T. Fukushima, and T. Okoshi, "Stripe structure dependence of frequency modulation characteristics of AlGaAs lasers," *Electron. Lett.*, vol. 21, pp. 1088-1090, 1985.
[13] ——, "Frequency-modulation characteristics of semiconductor lasers: Deviation from theoretical prediction by rate equation analysis," *Electron. Lett.*, vol. 22, pp. 741-743, 1986.
[14] K. Vahala, L. C. Chiu, S. Margalit, and A. Yariv, "On the linewidth enhancement factor α in semiconductor injection lasers," *Appl. Phys. Lett.*, vol. 42, pp. 631-633, 1983.
[15] A. S. Sudbø, "Rate equation models and wavelength modulation in semiconductor diode lasers," *IEEE J. Quantum Electron.*, vol. QE-23, pp. 1127-1134, 1987.
[16] ——, "The frequency chirp of current modulated semiconductor diode lasers," *IEEE J. Quantum Electron.*, vol. QE-22, pp. 1006-1008, 1986.
[17] K. Furuya, "Dependence of the linewidth enhancement factor α on waveguide structure in semiconductor lasers," *Electron. Lett.*, vol. 21, pp. 200-201, 1985.
[18] J. Arnaud, "Role of Petermann's K-factor in semiconductor laser oscillators," *Electron. Lett.*, vol. 21, pp. 538-539, 1985.
[19] T. Okoshi, K. Kikuchi, and A. Nakayama, "Novel method for high resolution measurement of laser output spectrum," *Electron. Lett.*, vol. 16, pp. 630-631, 1980.

Owen Doyle was born in Nashville, TN, on August 5, 1962. He received the B.S. and M.S. degrees in electrical engineering from the Massachusetts Institute of Technology, Cambridge, in 1984, and the Diplôme de Docteur Ingénieur from the Ecole Nationale Supérieure des Telecommunications, Paris, France, in 1987.

Since 1984 he has been working in the optoelectronics group of the Ecole Nationale Supérieure des Télécommunications. His research involves the modeling and characterization of semiconductor laser for coherent optical communications systems.

Phillippe B. Gallion (M'82), photograph and biography not available at the time of publication.

Guy Debarge, photograph and biography not available at the time of publication.